Dalton Transactions

Accepted Manuscript

Volume 45 | Number 1 | 7 January 2016 | Pages 1–398

Dalton Transactions

An international journal of inorganic chemistry
www.rsc.org/dalton

ISSN 1477-9226

PAPER
Joseph T. Hupp, Omar K. Farha et al.
Efficient extraction of sulfate from water using a Zr-metal–organic framework

175 YEARS

ROYAL SOCIETY OF CHEMISTRY

rsc.li/dalton

Dalton Transactions

ARTICLE

Coordination chemistry of flexible benzene-1,3,5-tricarboxamide derived carboxylates; notable structural resilience and vaguely familiar packing motifs

Amy D. Lynes,[a]* Chris S. Hawes,[a,b] Kevin Byrne,[c] Wolfgang Schmitt[c] and Thorfinnur Gunnlaugsson[a]*
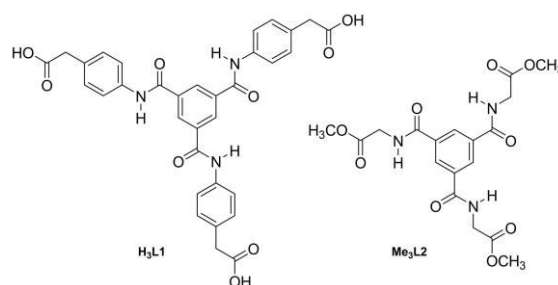
Flexible benzene-1,3,5-tricarboxamides (BTAs), organic species well-known for their tendencies to form functional soft-materials by virtue of their complementary hydrogen bonding, are explored as structurally reinforcing supramolecular building blocks in porous coordination polymers. We report the synthesis and characterisation of two related, carboxylate-terminated BTA derivatives, and the structure and functionality of their polymeric Cd(II) complexes. The polycarboxylate ligand benzene-1,3,5-tricarboxamide tris(phenylacetic acid) **H₃L1** was prepared, and the analogous trimethyl benzene-1,3,5-tricarboxamide tris acetate **Me₃L2** was prepared and its single crystal structure elucidated. On reaction with cadmium nitrate in a DMF/H₂O mixture, each BTA compound yielded coordination polymer species with significant solvent-accessible volume, and with columnar packing motifs comparable to the familiar BTA triple helix seen in purely organic systems. In the case of **Me₃L2**, this transformation was achieved through a convenient *in-situ* ester hydrolysis. Complex **1** is a 2-dimensional layered material containing tubular intralayer pores, in which amide-amide hydrogen bonding is a notable structural feature. In contrast, the structure of **2** contains no amide-amide hydrogen bonding, and instead a columnar arrangement of ligand species is linked by trinuclear Cd(II) cluster nodes into a densely packed three-dimensional framework. The crystal structures revealed both materials exhibited significant solvent-accessible volume, and this was probed with thermal analysis and CO_2 and N_2 adsorption experiments; complex **2** showed negligible gas uptake, while compound **1** possesses an unusually high CO_2 capacity for a two-dimensional material with intralayer porosity and surprising structural resilience to guest exchange, evacuation and exposure to air.

Introduction

Incorporating the principles of supramolecular chemistry into the design and synthesis of new functional materials is a current research area of great importance.[1] With the maturing of the underlying concepts, the opportunity now exists to harness weak and reversible intermolecular forces, for example hydrogen bonding, halogen bonding and π-π interactions,[2] to engineer additional structural or functional features within coordination polymer materials. Coordination polymers (of which Metal-Organic Frameworks are a sub-set) have been widely reported to exhibit properties useful for a diverse range of potential applications in gas separation and storage,[3, 4] sensing,[5] catalysis,[6] and various biomedical applications,[7] as well as continuously revealing unique fundamental properties.[8] A key consideration for future directions in the field is to construct such materials with additional backbone

functionalities, beyond those imparted purely by the metal ion and coordination environment. As well as a method for introducing structure-directing groups, ligand-based photoluminescence, catalytic sites and CO_2 chemisorption functionality have been introduced to great effect, providing a versatile route to multi-functional materials.[9]

Benzene-1,3,5-tricarboxamides (BTAs) are an important class of compounds in supramolecular chemistry.[10, 11] A broad range of readily-accessible BTA derivatives has allowed this class of molecules to act as a platform in many fundamental studies into the nature of molecular aggregation, with special relevance to soft materials.[12-15] Containing both hydrogen bond donor and acceptor sites, BTA derivatives can undergo 'supramolecular polymerisation' through intermolecular

a. *School of Chemistry and Trinity Biomedical Sciences Institute (TBSI), The University of Dublin, Trinity College Dublin, Dublin 2, Ireland*
b. *School of Chemical and Physical Sciences, Keele University, Keele ST5 5BG, United Kingdom*
c. *School of Chemistry & Centre for Research on Adaptive Nanostructures and Nanodevices, The University of Dublin, Trinity College Dublin, Dublin 2, Ireland.*

Scheme 1. Structure of **H₃L1** and **Me₃L2** developed in this study

ARTICLE

amide-amide hydrogen bonds and π-π stacking, forming a linear triple-helical structure both in the solid state and in solution. The amide substituents provide a synthetic handle for incorporating a diverse range of functionality in BTA derivatives, either retaining the natural C_3 symmetry or through unsymmetric substitution.[10] It has been widely demonstrated that the nature of the amide side chains has a great impact on the bulk properties of BTA materials.[12, 16] In particular, the dominant aggregation mode can be influenced away from the classic threefold hydrogen bonded helix in the presence of competing hydrogen bond donors or other directing forces, as we among others have recently demonstrated.[12-14, 17] Controlling the aggregation mode of BTA derivatives has been particularly important in directing the formation of discotic liquid crystalline mesophases,[18] as well as functional supramolecular gels, with columnar aggregation prominent in both instances.[12-14, 19]

As with most polytopic scaffolds, BTA derivatives have recently seen increasing use as ligands in coordination polymers and discrete metallocages. In the former, and keeping with conventional wisdom, rigid side chains are strongly represented,[20] along with amino acids,[17] while in the latter case, flexible chains terminated with *N*-donor ligands have been used to great success.[21] Underrepresented, however, are instances of extended structures from BTA derivatives with both large bridging distances between metal binding sites and inherent side-chain flexibility. Such systems could be expected to allow a more complex interplay of structure direction between the metal binding sites and the aggregation-prone core group, with neither influence strongly limited by the other, and sufficient spatial separation of the two key elements to allow for an extended structure dictated by two distinct synthons. Here, we report the synthesis and characterisation of two BTA derivatives, namely benzene-1,3,5-tricarboxamide tris(phenylacetic acid) **H₃L1**, and the analogous trimethyl benzene-1,3,5-tricarboxamide tris acetate **Me₃L2**, Scheme 1. These two have similar degrees of flexibility but substantially different bridging distances and the presence of three additional aromatic rings for intermolecular interactions in **L1**; the reaction of each with Cd(II), and the structural and physical properties of the resulting porous or non-porous constructs is described in full herein.

Results and discussion

Synthesis and structural studies

The syntheses of **H₃L1** and **Me₃L2** (See ESI and the Experimental section) were carried out based on established protocols for the symmetric tri-substitution of benzene-1,3,5-tricarbonyl trichloride, using methyl (4-aminophenyl) acetate hydrochloride and glycine methyl ester hydrochloride, respectively.[12, 14] **Me₃L1** was converted to the corresponding carboxylic acid by base hydrolysis followed by acidification to precipitate the neutral compound in good yield. In the case of **L2**, the subsequent coordination chemistry was more convenient in our hands using the methyl ester **Me₃L2** as a

feedstock, employing an *in-situ* hydrolysis reaction prior to coordination, often utilised in solvothermal synthesis.[22] Although many examples are known of symmetric BTA-derived gelators,[12, 19] especially with carboxylic acid termini,[14] we were unable to reliably generate any stable gels from **H₃L1** or the ester precursor, using a variety of different solvent mixtures and methods. This is most likely as a consequence of its relatively low solubility endowed by the aromatic linking groups. Similarly, we were unable to generate good quality single crystals of **Me₃L1** or **H₃L1** themselves for structure determination. The properties of **H₃L2/Me₃L2**, including gelation behaviour,[23] and some examples of coordination chemistry with first-row transition metals, alkali earth metals and lanthanides, have been reported elsewhere.[24] However, to provide a structural comparison, single crystals of **Me₃L2** were prepared by recrystallization from H₂O.
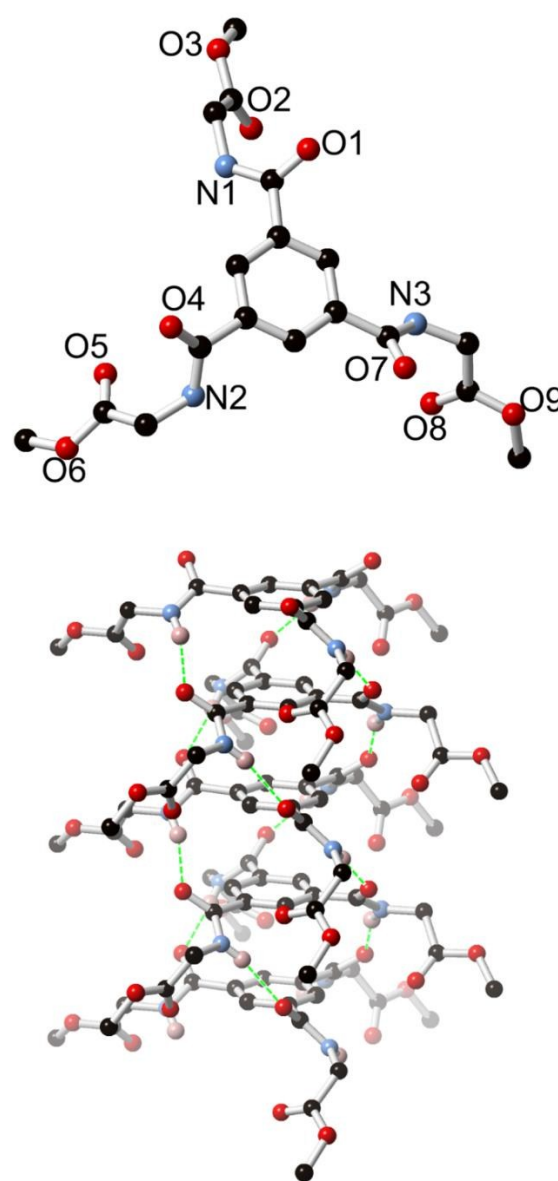
Figure 1 Structure of compound **Me₃L2**, showing (top) molecular structure with heteroatom labelling scheme, and (bottom) columnar stacking arrangement with triple-helical hydrogen bonding motif. Hydrogen atoms and ester group disorder are omitted for clarity.

Dalton Transactions

Structure of Me₃L2·0.5H₂O

A single crystal of **Me₃L2**, grown in water, was subjected to single crystal X-ray diffraction with the data obtained solved and the structural model refined in the monoclinic space group $P2_1/n$. The asymmetric unit contains one complete molecule of the title compound. Two partial-occupancy H₂O sites were located within the asymmetric unit (total occupancy 0.5), and minor disorder was evident for one of the three methyl ester groups. The BTA core, as shown in Figure 1, exhibits approximate C₃ symmetry with each amide group adopting the typical *ca.* 40° offset to the phenyl ring mean plane. This arrangement leads to the expected triple-helical hydrogen bonding arrangement of adjacent molecules, which align parallel to the *b* axis with three N-H···O hydrogen bonds between each unit, and an interplanar distance between adjacent phenyl rings of 3.469(2) Å, half the length of the *b* unit cell edge. Adjacent phenyl rings are parallel and essentially co-axial, slipped by only 0.3 Å to one another. The methyl ester groups protrude from these helical stacks and interdigitate between adjacent columns, which align in a typical hexagonal rod packing motif. X-ray powder diffraction (See ESI) confirmed that the bulk material consists of a single phase which is described by the structural model. This observation confirms that the extended structure of **Me₃L2** conforms to the standard BTA packing model when crystallised in the absence of any strongly competing hydrogen bonding or other intermolecular interactions.

Structural chemistry of Cd(II) complexes of L1 and L2

In order to examine the competitive influences of metal binding and core hydrogen bonding on extended frameworks containing **L1** and **L2**, Cd(II) was chosen as an appropriate metal ion for this study, having good affinity for carboxylate donors in 6 to 8-coordinate bonding modes, yet no strong energetic preference for particular coordination geometries. These tendencies maximise the likelihood of forming robust coordination frameworks where influences besides coordination geometry are likely to have significant impact. To this end, **H₃L1** and **Me₃L2** were each reacted with cadmium nitrate tetrahydrate in 1:1 DMF:H₂O mixtures at 100 °C, each providing colourless crystals within 24 hours.

Structure of [Cd₃(L1)₂(DMF)₂]·5H₂O·2DMF 1

Complex **1** was analysed by single crystal X-ray diffraction at 100 K, with the data solved and the structural model refined in the triclinic space group *P*-1. The asymmetric unit contains three unique cadmium environments and two complete **L1** species, with each carboxylate deprotonated. A small proportion of disorder in the vicinity of cadmium sites Cd2 and Cd3 were observed, with the second component refining to an occupancy of 15%; for the purposes of this discussion, only the major component will be discussed. Further details are provided as electronic supporting information (See ESI).

The coordination spheres of each of the three unique cadmium ions were filled by oxygen donors, either from **L1** carboxylates or two unique DMF ligands, as shown in Figure 2.

Cadmium ion Cd1 adopts a 7-coordinate geometry, while Cd2 and Cd3 both exhibit distorted octahedral 6-coordinate geometries. As is regularly observed in Cd-carboxylate systems, bridging coordination modes are widely adopted here; Cd1-Cd2 and Cd2-Cd3 are each bridged by three unique carboxylates, while Cd3-Cd1 are doubly bridged. This bridging leads to a one-dimensional cadmium-carboxylate chain which extends parallel to the *a* axis. Of the six unique carboxylate groups in the asymmetric unit, three instances of μ₂-κO,O':κO coordination are present, with two instances of μ₂-κO:κO' bridging and one example of μ₃-κO:κO:κO' coordination (Figure 2). The Cd-Cd distances are 3.6168(6), 3.7528(7) and 3.7205(6) Å for Cd1-Cd2, Cd2-Cd3 and Cd3-Cd1, respectively, and (although somewhat less reliable due to the necessary disorder modelling), all bonding Cd-O distances fall in the range 2.187(4) Å (Cd1-O1) to 2.503(4) Å (Cd1-O6).
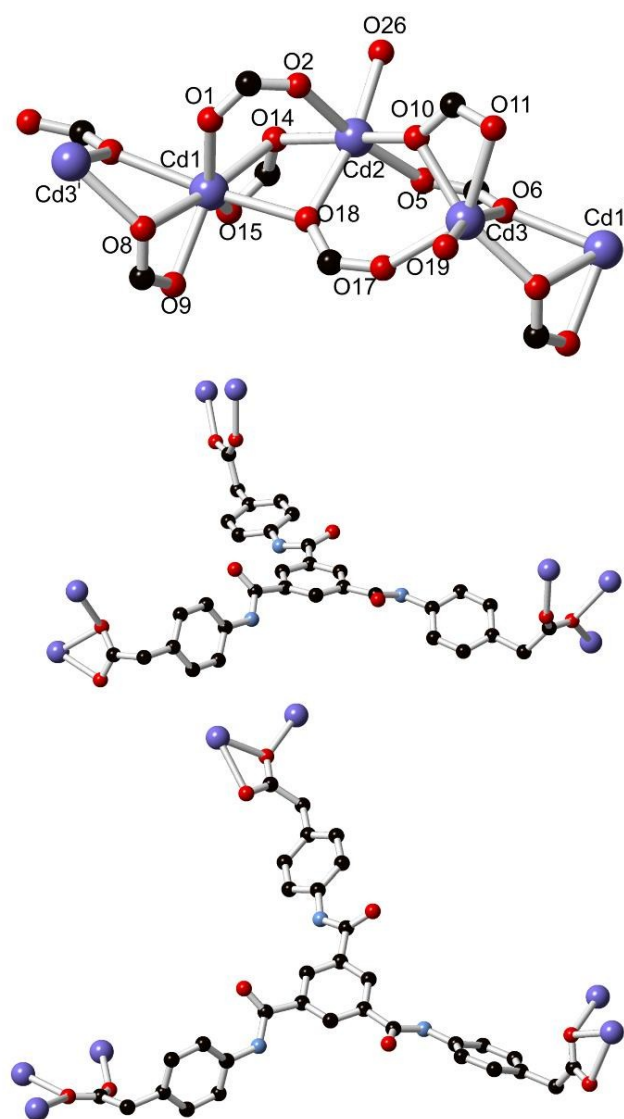
Figure 2 Connectivity and chemical environment of the three nodes in complex **1**; (Top) Cadmium coordination geometry with heteroatom labelling scheme, where O26 corresponds to a coordinating DMF molecule; (Middle/Bottom) Connectivity of the two crystallographically independent **L1** molecules within the structure. Hydrogen atoms, framework disorder, lattice solvent molecules and selected atom labels are omitted for clarity. Symmetry codes used to generate equivalent atoms: (i) –x, 1-y, 2-z; (ii) 1-x, 1-x, 2-z.

The **L1** species in the structure of **1** adopt a splayed T-shaped conformation and the two crystallographically unique moieties alternate in a stack aligned parallel to the *a* axis and parallel to the cadmium-carboxylate chains. The two species exhibit similar conformations with the slight differences mainly manifested in variations in the orientation of the acetate fragments. While adjacent molecules align into slipped stacks, the traditional BTA hydrogen bonding mode is not observed between directly adjacent molecules in this fashion; only three of a possible six unique amide-amide hydrogen bonds are observed in each stack. As shown in Figure 3, while the adjacent BTA ring planes are separated by *ca.* 3.2 Å in the direction of the plane normal vector, the rings are horizontally slipped by *ca* 3.7 Å, further distinguishing this packing mode from the typical BTA helix. The amide N-H groups not involved in amide-amide hydrogen bonding fulfil their hydrogen bonding requirements with lattice DMF molecules (two instances) and a lattice water molecule.
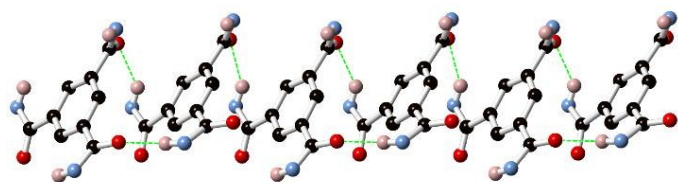

Figure 3 Hydrogen bonding interactions between alternating adjacent core units of **L1** molecules in the structure of complex **1**, showing the slipped-stack packing arrangement.

The T-shaped conformation of the **L1** molecules linking one-dimensional cadmium-carboxylate chains gives rise to a corrugated double-layer two-dimensional framework, oriented parallel to the *ac* plane and represented in Figure 4. Within each sheet, two crystallographically independent, rectangular intralayer solvent channels are present with maximum interatomic dimensions *ca.* 12.5 × 8 Å (omitting solvent molecules). In the crystallographic model, a total of 5 DMF (2 coordinating, 3 non-coordinating) sites were located, with total occupancy of 4.2 DMF molecules per 3 cadmium ions, and three unique water sites with total occupancy 2.5 molecules per 3 cadmium ions. It is expected that further DMF sites were present within the structure, associated with the 15% disorder contribution of two cadmium sites, however these could not be sensibly modelled (See ESI). Adjacent layers associate in the *b* direction through various π···π and C-H···π interactions, as well as a defined hydrogen bonding interaction through lattice water molecules between cadmium-carboxylate chains of adjacent sheets. While all solvent molecules were included in the final refinement, removal of the lattice solvent from the model gave an estimate of 25% solvent accessible volume (probe radius 1.2 Å), which was mostly localised in the intralayer channels with a small contribution from narrow channels between adjacent layers.
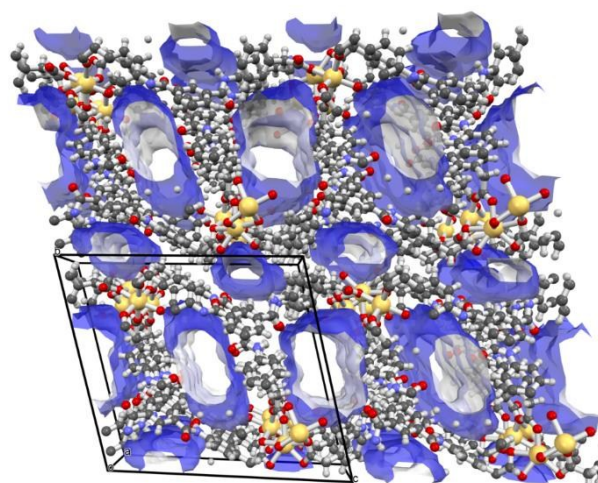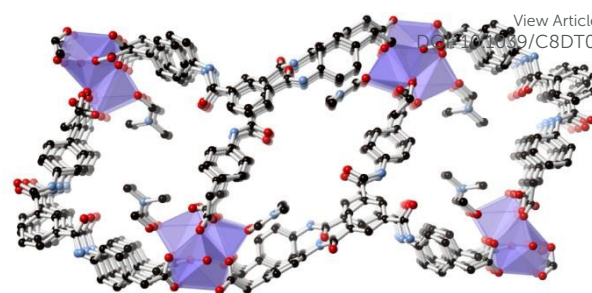

Figure 4 The extended structure and solvent-accessible voids in complex **1**; (Top) structure of an individual network of **2** showing the 1-dimensional intralayer solvent channels (non-coordinating solvent molecules omitted); (Bottom) the 3-dimensional structure of **1** showing the intralayer void volume and smaller interlayer pores.

Structure of [Cd$_3$(L2)$_2$(DMF)(H$_2$O)$_3$]·5(H$_2$O) 2

A crystal of complex **2** was subjected to single crystal X-ray diffraction, with the data solved and the structural model refined in the monoclinic space group *P*2$_1$/*c*. The structure of **2** contains three unique cadmium environments and two unique ligands within the asymmetric unit, and confirms hydrolysis of the ester groups of **Me$_3$L2** during the synthesis. All six independent carboxylate groups undergo coordination to cadmium ions, with the cadmium coordination spheres completed by one coordinating amide oxygen atom (O16), 3 unique aqua ligands, and one DMF ligand. Each of the three cadmium ions adopts a unique coordination number and geometry, with 6-, 7- and 8-coordinate geometries represented by cadmium ions Cd1, Cd2 and Cd3, respectively. The metal coordination environment is best described as a trinuclear cluster node, where the metal centres are linked by four bridging carboxylate groups, as shown in Figure 5. Three of these groups adopt a μ$_2$-κO,O':κO binding mode, with the remainder engaged in a triply-bridging μ$_3$-κO:κO:κO' coordination mode. The other two carboxylate groups adopt purely chelating coordination modes. Around the immediate periphery of the trinuclear cluster environment, numerous O-H···O hydrogen bonds (originating from the aqua ligands) and N-H···O hydrogen bonds from adjacent amide groups serve to further support the cluster geometry.

The extended structure of complex **2** is a densely connected 3-dimensional coordination polymer. Topologically, the

Dalton Transactions

ARTICLE

connectivity cannot be easily related to a known net; the obvious choice of nodes (the cadmium cluster and each of the two ligands) gives a 3,4,7-connected trinodal topology with the point symbol $(4\cdot6^2)(4^3\cdot6^3)(4^4\cdot6^{14}\cdot8^3)$, shown in Figure 6.[25] This complexity largely comes as a result of the coordination from the amide oxygen of one of the two unique ligand species, giving different connectivity to the two ligand nodes. Nonetheless, disregarding this interaction does not restore symmetry between the two nodes and fails to simplify the network description.
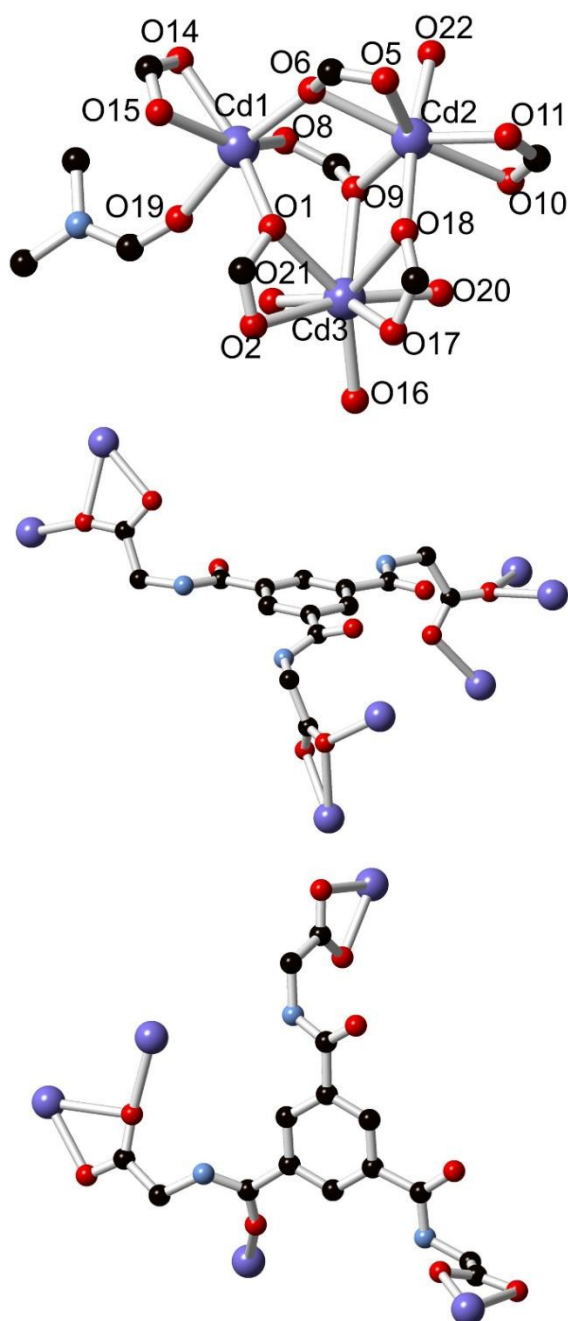

Figure 5 Connectivity and chemical environment of the three nodes in the structure of **2**. Top: the coordination sphere of the trinuclear cadmium node, with atom labelling scheme; Bottom: connectivity of the two unique **L2** groups. Hydrogen atoms and atom labels are omitted for clarity.

The structure of **2**, in comparison to **1** and other BTA-containing structures, contains no amide-amide hydrogen bonding. Instead, five N-H hydrogen bond donors are occupied in hydrogen bonds to carboxylate oxygen atoms, and one instance of an N-H···O hydrogen bond to a lattice water molecule is present. This behaviour is comparable to structural properties we have previously observed in short-chain BTA carboxylate species where competitive hydrogen bonding functionality is present.[12] Interestingly, however, the BTA core groups of **L2** are still aligned in stacks in the structure of **2** despite the absence of amide-amide interactions. These columns, aligned parallel to the *a* axis, proceed in an AABBAA fashion with respect to the two unique ligand molecules, and are supported by N-H···O(carboxylate) hydrogen bonds at their periphery. Each aromatic core is separated by 3.66, 3.77 and 3.59 Å for the two symmetric and one unsymmetric pairings, respectively, while the ring centroids are slipped by 0.4 – 0.6 Å for the symmetric pairings and 1.6 Å for the unsymmetric. Considering these columns as structural features, the extended network can be described as an approximately hexagonal rod packing motif, where each column is connected to one another through six sets of radially distributed cadmium cluster nodes as shown in Figure 6.

In addition to the DMF and aqua ligands within the asymmetric unit, the structure of **2** also contains a total of five lattice water molecules; minor crystallographic disorder required modelling these over a total of seven positions. Primarily these species take part in hydrogen bonding interactions with one another and the aqua ligands and carboxylate groups within the structure. The arrangement of these groups forms narrow one-dimensional channels parallel to the crystallographic *c* axis and perpendicular to the propagation of the BTA stacks. These unbound water molecules account for an approximate solvent-accessible volume of 9%, increasing to 21% when considering metal-bound solvent molecules (probe radius 1.2 Å).

Thermal properties and gas adsorption

As the structures of complexes **1** and **2** both contained significant and continuous regions of lattice solvent, thermogravimetric analysis (TGA) was carried out on each material to ascertain the ideal conditions for desolvation and subsequent guest uptake. The as-synthesised complex **1** exhibited a multi-step desolvation and decomposition profile, with a mass loss of approximately 30 % before 70 °C and a further 10 % before 150 °C, before gradually stabilising before the onset of decomposition at *ca.* 350 °C. The total volatile mass of *ca.* 40% corresponds to the combination of the crystallographically-resolved DMF and H_2O guests, as well as additional surface solvent from the freshly-isolated crystals. Soaking the crystals in MeCN for 48 hours facilitated guest exchange, yielding a phase which could be mostly desolvated near room temperature, with the thermogravimetric analysis curve flattening above 100 °C. X-ray powder diffraction revealed the solvent-exchanged and air dried material retained an equivalent framework structure to the as-synthesised

ARTICLE

material. In comparison, TGA of a freshly prepared sample of complex **2** revealed a steep mass loss of approximately 25 % before 100 °C, flattening before the onset of decomposition at approximately 300 °C. The tendency of **2** to readily desolvate on heating suggested that solvent exchange was unnecessary to achieve activation at moderate temperatures.

Figure 6 Extended structure of complex **2**; (Top) the linear stacks of **L2** groups encircled by trinuclear cadmium clusters; (Bottom) topological representation of the network viewed parallel to the stacks; yellow represents **L2** nodes and pink represents cadmium clusters.

Following solvent exchange with MeCN, a sample of complex **1** was activated under dynamic vacuum at 100 °C for 24 hours, and the internal pore volume was characterised using CO_2 and N_2 as probe molecules. Relatively minor uptake of N_2 was observed at 77 K (*ca.* 6 cc(STP)/g) from microporous

features in the pressure range P/P_0 0 – 0.01 followed by a shallow monotonic increase to P = 0.99P_0 up to a maximum loading of 14 cc(STP)/g. This low-capacity type I behaviour (with calculated BET surface area of *ca.* 5 m^2/g, ESI) indicates poor affinity of the host for the N_2 probe molecule under these conditions. Adsorption of CO_2 at 278K yielded much greater uptake, with a total adsorption capacity of 103 cc(STP)/g (17 wt%) at 1 bar, shown in Figure 7. Surface area calculations from these data using the Dubinin-Radushkevich method yielded a surface area at 278 K of 207 m^2/g (ESI), a figure more consistent with the microporous features apparent from the single crystal structure. This selectivity likely arises from the relatively narrow and polar micropores present in **1**, expected to favour the larger quadrupole of CO_2 compared to N_2. The smooth adsorption and desorption curves, with minor hysteresis, show no obvious indication of framework flexibility or reorganisation during the adsorption process.
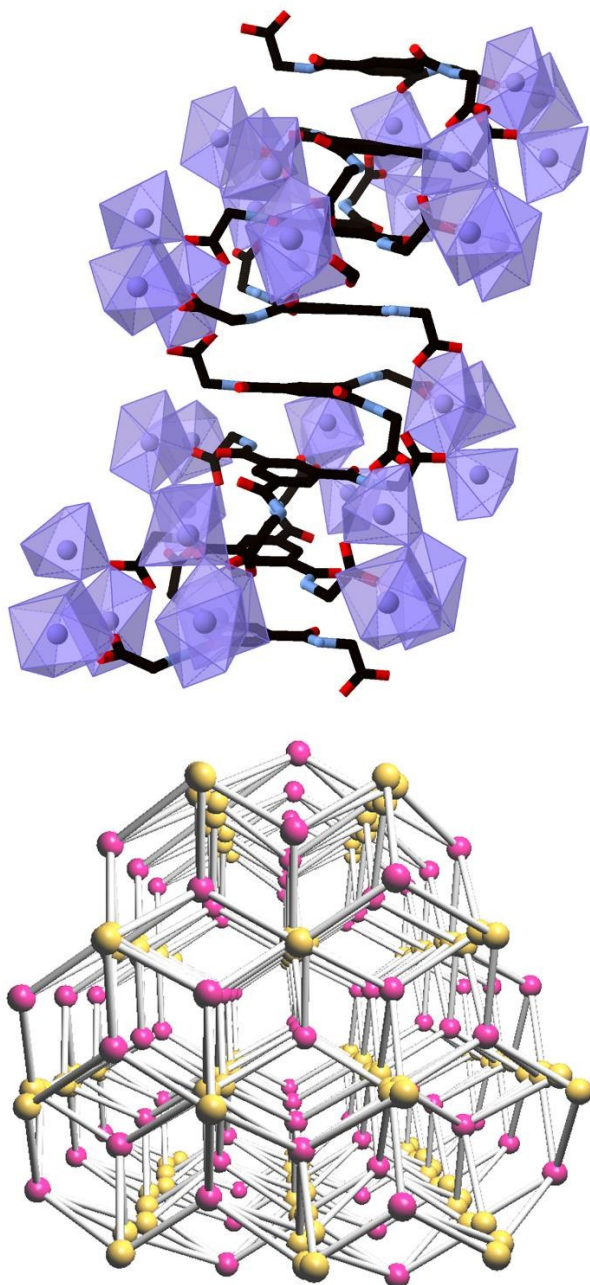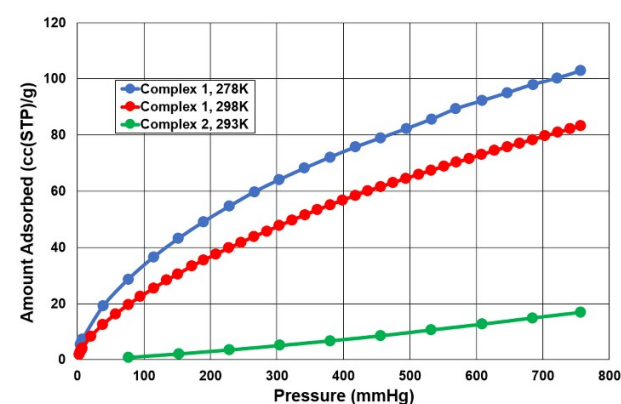

Figure 7 CO_2 adsorption isotherms for complex **1** (blue/red, 278 K and 298 K, respectively) and complex **2** (green, 293 K) showing the marked differences in CO_2 uptake performance between the two materials.

Repeating the adsorption cycle at 293 K gave a similar curve with maximum capacity of 83 cc(STP)/g at 1 bar. Fitting the datapoints from the two adsorption cycles with a virial-type model using the Clausius-Clapyeron relation (See ESI), the enthalpy of adsorption across the loading range was estimated. Shown in Figure S13 (See ESI), the zero-loading enthalpy of adsorption for CO_2 is estimated at approximately -28 kJ mol^{-1}, reaching a plateau value of approximately -23 kJ mol^{-1} at higher loadings. These values are consistent with those typically observed for physisorption onto organic pore walls with modest polarity, suggesting little direct interaction from the metal sites or potential hydrogen bond donors in the adsorption process. Although the preferential adsorption of CO_2 at 278K over N_2 at 77K is not surprising for a microporous material, the CO_2 capacity shown by **1** under mild conditions is unusually high for a 2-dimensional framework showing only intralayer porosity; the capacity at 293 K / 1 bar is comparable to that shown by well-known 3-dimensional materials including HKUST-1, MIL-53(Al) and UiO-66.[3, 26]

Complex **2** was also examined for gas uptake, with evacuation of the freshly isolated material carried out at 100 °C under dynamic vacuum overnight. In contrast to complex **1**, however, both CO_2 (293 K) and N_2 (77 K) adsorption experiments showed negligible adsorption. N_2 uptake fell below

the instrumental detection limit, while CO_2 adsorption reached a maximum loading of only *ca.* 17 cc(STP)/g at 1 bar with no obvious inflection point in the adsorption branch, both consistent with adsorption on the external particle surfaces only. In the case of both complexes **1** and **2**, X-ray powder diffraction following gas adsorption showed that crystalline materials closely related in structure to the freshly synthesised compounds were recovered following exposure to air.

Discussion

Comparing the structures of **1** and **2**, it is clear that, while neither adopts the triple-helical columnar stacking arrangement present in **Me₃L2** and many other BTA compounds, slipped columnar packing arrangements are nonetheless dominant in their extended structures. Although in the case of complex **2** no amide-amide hydrogen bonding interactions were present to facilitate this, the short distance between the BTA amide groups and the terminal carboxylate oxygen atoms ensured a small separation between the core segments of adjacent molecules. In the case of complex **1**, the significant slippage between the core groups of each ligand molecule was a further deviation from typical behaviour, although the amide-amide hydrogen bonding interactions were present for half of the amide groups within the asymmetric unit. Complex **1** also benefits from three additional aromatic groups per BTA group to facilitate more significant π-π interactions. The fate of the remaining three amide N-H groups, which decorate both the inter- and intra-layer channels, following solvent exchange and evacuation is uncertain. The CO_2 adsorption enthalpy at zero loading is not indicative of strong N-H⋯OCO interactions which would be anticipated if the structure is invariant following solvent removal. This may be consistent with a structural rearrangement on evacuation in which these hydrogen bonding interactions are satisfied by other framework acceptors.

The variation in guest capacity after degassing between compounds **1** and **2** is not especially surprising, given their variation in bridging distances and resulting differences in pore dimensions. However, more unusual is the excellent CO_2 capacity for complex **1** despite its two-dimensional structure; many similar systems have previously been implicated in structural collapse following evacuation.[27] The poor gas uptake performance for compound **2** may be rationalised by a combination of the restricted pore size as well as, conceivably, a greater freedom of ligand flexibility bought about from the discrete cadmium-carboxylate cluster nodes, compared to the more inter-connected cadmium-carboxylate columns in complex **1**. Both complexes were prepared in a substantially hydrated form, evidenced by resolved hydrogen-bonded solvent networks in both crystal structures. As such, regeneration of similar crystalline phases to the pristine materials after exposure of the evacuated samples to air is seemingly consistent with reformation of hydrogen bonding interactions between atmospheric water molecules and the internal pore walls.

Conclusion

We have prepared two new BTA-derived cadmium(II) coordination polymers, namely [Cd₃(**L1**)₂(DMF)₂]·5H₂O·2DMF **1** and

[Cd₃(**L2**)₂(DMF)]·5(H₂O) **2**, and described their structural and thermal properties and capacity for gas uptake. Both compounds form extended networks through polynuclear cadmium-carboxylate building units, and hydrogen bonding interactions through the BTA amide groups provide additional structure direction. While both materials could be thermally desolvated (following solvent exchange in the case of **1**), only **1** showed appreciable CO_2 uptake. The CO_2 capacity at 1 bar / 278 K of 17 wt% is unusually high for a two-dimensional material, particularly one derived from a flexible ligand, and indicates the combined structural resilience of the interconnected cadmium-carboxylate rod building units and hydrogen bonding interactions within the framework. The study of BTA-derived coordination polymers, both crystalline and amorphous, and the interplay of their coordination and hydrogen bonding interactions is a fascinating route towards novel functional materials, which we hope will continue to develop in the future.

Experimental

Materials and methods

All reagents and solvents were purchased from Sigma-Aldrich, Fisher Scientific or TCI Ltd, were of reagent grade or better, and were used without further purification unless otherwise stated. Where necessary, solvents were dried over activated alumina using an Innovative Technology PureSolv solvent purification system. Electrospray ionisation mass spectra were recorded on a Mass Lynx NT V 3.4 on a Waters 600 controller connected to a 996 photodiode array detector with HPLC-grade CH_3CN or CH_3OH as carrier solvents. Infrared spectra were recorded in the range 4000-650 cm⁻¹ on a Perkin-Elmer Spectrum One FT-IR spectrometer equipped with a Universal ATR sampling accessory. NMR data were recorded on a Bruker-DPX-400-Avance spectrometer (400.13 (¹H) and 100.6 (¹³C) MHz) and on a Bruker AV-600 spectrometer (600.13 (1H) and 150.2 (13C) MHz) in commercially available deuterated solvents. Chemical shifts are reported in ppm relative to SiMe4 (= 0 ppm) and referenced relative to the internal solvent signals. Data were processed with Bruker Win-NMR 5.0, Topspin and MestReNova softwares. Melting point measurements were carried out using an electrothermal 1A900 melting point apparatus in an unsealed capillary tube. Elemental analysis was carried out on Exeter Analytical CE440 elemental analyser at the microanalysis laboratory, School of Chemistry and Chemical Biology, University College Dublin. Thermogravimetric (TGA) analysis was carried out with a Perkin-Elmer Pyris 1 thermogravimetric analyser. Samples were spread on alumina crucibles and heated under nitrogen purge flow of 20 ml/min at a heating rate of 5 °C/min. Gas adsorption isotherms were measured using a Quantachrome Autosorb IQ gas sorption analyser. Chemically pure (CP, N4.5) grade He, N₂, H₂ and CO_2 gases were used for the measurements.

X-Ray Crystallography and powder diffraction

ARTICLE

Structural and refinement parameters are presented in Table 1. All diffraction data were collected using a Bruker APEX-II Duo dual-source instrument using microfocus Cu Kα (λ = 1.54178 Å) radiation. Datasets were collected using ω and φ scans with the samples immersed in oil and maintained at a constant temperature of 100 K using a Cobra cryostream. The data were reduced and processed using the Bruker APEX suite of programs.[28] Multi-scan absorption corrections were applied using SADABS.[29] The diffraction data were solved using SHELXT and refined by full-matrix least squares procedures using SHELXL-2015 within the OLEX-2 GUI.[30] The functions minimized were $\Sigma w(F^2_o - F^2_c)$, with $w = [\sigma^2(F^2_o) + aP^2 + bP]^{-1}$, where $P = [\max(Fo)2 + 2F2c]/3$. All non-hydrogen atoms were refined with anisotropic displacement parameters. All carbon-bound hydrogen atoms were placed in calculated positions and refined with a riding model, with isotropic displacement parameters equal to either 1.2 or 1.5 times the isotropic equivalent of their carrier atoms. In the case of complex **1**, meaningful disorder was detected in the vicinity of two of the three unique cadmium sites which necessitated partial disorder modelling of the surrounding groups, details are given as supporting information. Other specific refinement strategies are outlined in the refine_special_details section of the combined crystallographic information file (cif) where appropriate. CCDC 1812950-1812952. X-ray powder diffraction patterns were collected using a Bruker D2 Phaser instrument with Cu Kα radiation (λ = 1.5418 Å). Samples were ground and mounted on silicon sample holders, and data were collected in the 2θ range 5 – 55° at room temperature.

Synthesis

Experimental procedures for the synthesis of methyl 2-(4-aminophenyl)acetate and Me₃L1 are provided as electronic supporting information (ESI)

Synthesis of benzene-1,3,5-tri(carboxamide) tris phenyl acetic acid H₃L1

The ester precursor (Me₃L1) was dissolved in 5 ml CH₃OH, cooled on ice and 5 equivalents of NaOH was added dropwise. The resulting solution was left to stir at room temperature for 6 hr. Acetic acid was added dropwise until the formation of a beige precipitate occurred. This was then filtered and washed with H₂O, with the resulting white solid dried in vacuo. 83 %; mp 250-260 °C; δ_H (DMSO-d₆, 600 MHz) 10.56 (d, 3H, NH), 8.67 (s, 3H, Aromatic), 7.74 (d, $J = 8.4$ Hz, 6H, Aromatic), 7.27 (d, $J = 8.28$ Hz, 6H, Aromatic), 3.53 (s, overlapping with H₂O signal, CH₂); δ_C (DMSO-d₆, 150 Hz) 172.9 (RCOOCH₃), 164.6 (RCONH), 137.6 (Aromatic), 135.6 (Aromatic), 130.8 (Aromatic), 129.7 (Aromatic), 120.5 (Aromatic), 40.1 (CH₂); m/z (HRMS-ESI⁻) [M-H]⁻ calcd for C₃₃H₂₇N₃O₉, 608.1669, found 608.1663; ν_{max} (cm⁻¹): 3316, 3070, 1707, 1647, 1603, 1533, 1513, 1412, 1322, 1221, 1192, 1168, 1020, 905, 809, 662.

Synthesis of trimethyl (1,3,5-tri(carboxamide)) tris methyl propionate Me₃L2

Glycine methyl ester hydrochloride (1.67g, 13 mmol) was dissolved in dry DCM (50 mL), then cooled in ice before the addition of Et₃N (2.52 g, 3.3 mL, 18 mmol). 1,3,5-Benzenetricarbonyl trichloride (1 g, 3.7 mmol) was added to the mixture and it was then stirred under argon at room temperature for 24 hr. The solution was washed with NaHCO₃ solution in H₂O three times, with organic layer collected and evaporated to reveal a pale whitish/yellow solid (0.79 g, 1.9 mmol, 50.4 %); mp 182-186 °C; δ_H (DMSO-d₆, 400 MHz) 9.22 (t, $J = 5.7$ Hz, 3H, NH), 8.48 (s, 3H, Aromatic), 4.04 (d, $J = 5.8$ Hz, 6H, CH₂), 3.64 (s, 9H, CH₃); δ_C (DMSO-d₆, 100 MHz) 170.2 (RCOOCH₃), 165.8 (CONH), 134.4 (Aromatic), 129 (Aromatic), 51.8 (OCH₃), 41.3 (CH₂); m/z (HRMS-ESI⁻) [M-H]⁻ calcd for C₁₈H₂₀N₃O₉, 422.12, found 422.1192; ν_{max} (cm⁻¹): 3245, 3069, 2951, 1752, 1641, 1563, 1436, 1400, 1362, 1310, 1203, 1091, 1027, 973, 920, 796, 689.

Synthesis of [Cd₃(L1)₂(DMF)₂]·5H₂O·2DMF

Cadmium nitrate tetrahydrate (15 mg, 48 μmol) and **L1** (10 mg, 16 μmol) were dissolved in DMF/H₂O (1:1, 3 mL), The reaction was sealed in a Teflon capped vial and heated at 100 °C for 24 hr. The resulting crystals were isolated by filtration to give **Cd-L1**. Mp (decomp) > 300 °C; Found C, 48.47; H, 4.06; N, 7.24, Calc. for C₆₆H₄₈Cd₃N₆O₁₈·5H₂O·4DMF: C, 48.47; H, 4.49; N, 7.25 %; ν_{max} (cm⁻¹): 3267, 2928, 1652, 1603, 1564, 1531, 1513, 1437, 1384, 1319, 1281, 1254, 1202, 1095, 1061, 1022, 927, 861, 815, 794, 751, 735, 715, 698, 679, 658. Phase purity was established by X-ray powder diffraction.

Synthesis of [Cd₃(L2)₂(DMF)(H₂O)₃]·5(H₂O)

Cadmium nitrate tetrahydrate (15 mg, 48 μmol) and **L2** (10 mg, 24 μmol) were dissolved in DMF/H₂O (1:1, 3 mL), The reaction was sealed in a Teflon capped vial and heated at 100 °C for 24 hr. The resulting crystals were isolated by filtration to give **Cd-L2**. Mp (decomp) > 300°C; Found C, 30.20; H, 3.19; N, 7.30, Calc. for C₃₃H₄₇Cd₃N₇O₂₇: C, 30.23; H, 3.61; N, 7.48 %; ν_{max} (cm⁻¹): 3327, 2938, 1652, 1593, 1531, 1430, 1390, 1288, 1269, 1092, 1003, 931, 904, 711, 664, 560. Phase purity was established by X-ray powder diffraction.

Conflicts of interest

There are no conflicts to declare.

Acknowledgements

Notes and references

View Article Online
DOI: 10.1039/C8DT00439K

1. I. V. Kolesnichenko and E. V. Anslyn, *Chem. Soc. Rev.*, 2017, **46**, 2385-2390; E. J. Howe, B. O. Okesola and D. K. Smith, *Chem. Commun.*, 2015, **51**, 7451-7454; D. B. Amabilino, D. K. Smith and J. W. Steed, *Chem. Soc. Rev.*, 2017, **46**, 2404-2420; C. D. Jones and J. W. Steed, *Chem. Soc. Rev.*, 2016, **45**, 6546-6596; A. J. Savyasachi, O. Kotova, S. Shanmugaraju, S. J. Bradberry, G. M. Ó'Máille and T. Gunnlaugsson, *Chem*, 2017, **3**, 764-811.

2. C. Kulkarni, E. W. Meijer and A. R. A. Palmans, *Acc. Chem. Res.*, 2017, **50**, 1928-1936; L. J. McCormick and D. R. Turner, *CrystEngComm*, 2013, **15**, 8234-8236; D. E. Barry, C. S. Hawes, S. Blasco and T. Gunnlaugsson, *Cryst. Growth Des.*, 2016, **16**, 5194-5205.

3. K. Sumida, D. L. Rogow, J. A. Mason, T. M. McDonald, E. D. Bloch, Z. R. Herm, T.-H. Bae and J. R. Long, *Chem. Rev.*, 2012, **112**, 724-781.

4. J.-R. Li, R. J. Kuppler and H.-C. Zhou, *Chem. Soc. Rev.*, 2009, **38**, 1477-1504.

5. E. M. Boyle, S. Comby, J. K. Molloy and T. Gunnlaugsson, *The Journal of Organic Chemistry*, 2013, **78**, 8312-8319; L. E. Kreno, K. Leong, O. K. Farha, M. Allendorf, R. P. Van Duyne and J. T. Hupp, *Chem. Rev.*, 2012, **112**, 1105-1125; W. P. Lustig, S. Mukherjee, N. D. Rudd, A. V. Desai, J. Li and S. K. Ghosh, *Chem. Soc. Rev.*, 2017, **46**, 3242-3285.

6. L. N. Neumann, M. B. Baker, C. M. A. Leenders, I. K. Voets, R. P. M. Lafleur, A. R. A. Palmans and E. W. Meijer, *Organic & Biomolecular Chemistry*, 2015, **13**, 7711-7719; D. Farrusseng, S. Aguado and C. Pinel, *Angew. Chem. Int. Ed.*, 2009, **48**, 7502-7513.

7. E. M. Surender, S. J. Bradberry, S. A. Bright, C. P. McCoy, D. C. Williams and T. Gunnlaugsson, *J. Am. Chem. Soc.*, 2017, **139**, 381-388; X. Du, J. Zhou, J. Shi and B. Xu, *Chem. Rev.*, 2015, **115**, 13165-13307; A. C. McKinlay, R. E. Morris, P. Horcajada, G. Férey, R. Gref, P. Couvreur and C. Serre, *Angew. Chem. Int. Ed.*, 2010, **49**, 6260-6266.

8. H. Furukawa, K. E. Cordova, M. O'Keeffe and O. M. Yaghi, *Science*, 2013, **341**; R. Ricco, C. Pfeiffer, K. Sumida, C. J. Sumby, P. Falcaro, S. Furukawa, N. R. Champness and C. J. Doonan, *CrystEngComm*, 2016, **18**, 6532-6542.

9. S. Kaskel, *Introduction*, Wiley-VCH Verlag GmbH & Co. KGaA, Weinheim, 2016.

10. S. Cantekin, T. F. A. de Greef and A. R. A. Palmans, *Chem. Soc. Rev.*, 2012, **41**, 6125-6137.

11. X. Lou, R. P. M. Lafleur, C. M. A. Leenders, S. M. C. Schoenmakers, N. M. Matsumoto, M. B. Baker, J. L. J. van Dongen, A. R. A. Palmans and E. W. Meijer, *Nature Communications*, 2017, **8**, 15420.

12. A. D. Lynes, C. S. Hawes, E. N. Ward, B. Haffner, M. E. Mobius, K. Byrne, W. Schmitt, R. Pal and T. Gunnlaugsson, *CrystEngComm*, 2017, **19**, 1427-1438.

13. O. Kotova, R. Daly, C. M. G. dos Santos, M. Boese, P. E. Kruger, J. J. Boland and T. Gunnlaugsson, *Angew. Chem. Int. Ed.*, 2012, **51**, 7208-7212.

14. R. C. T. Howe, A. P. Smalley, A. P. M. Guttenplan, M. W. R. Doggett, M. D. Eddleston, J. C. Tan and G. O. Lloyd, *Chem. Commun.*, 2013, **49**, 4268-4270.

15. A. Paikar, A. Pramanik and D. Haldar, *RSC Adv.*, 2015, **5**, 31845-31851; R. Daly, O. Kotova, M. Boese, T. Gunnlaugsson and J. J. Boland, *ACS Nano*, 2013, **7**, 4838-4845; A. Sakamoto, D. Ogata, T. Shikata, O. Urakawa and K. Hanabusa, *Polymer*, 2006, **47**, 956-960; T. Shikata, D. Ogata and K. Hanabusa, *J. Phys. Chem. B*, 2004, **108**, 508-514.

16. A. Desmarchelier, B. G. Alvarenga, X. Caumes, L. Dubreucq, C. Troufflard, M. Tessier, N. Vanthuyne, D. Maistriaux, D. Beljonne, P. Brocorens, R. Lazzaroni, M. Raynal and L. Bouteiller, *Soft Matter*, 2016, **12**, 7824-7838; P. J. M. Stals, J. F. Haveman, R. Martin-Rapun, C. F. C. Fitie, A. R. A. Palmans and E. W. Meijer, *J. Mater. Chem.*, 2009, **19**, 124-130.

17. P. Jana, A. Paikar, S. Bera, S. K. Maity and D. Haldar, *Org. Lett.*, 2014, **16**, 38-41.

18. C. F. C. Fitié, W. S. C. Roelofs, P. C. M. M. Magusin, M. Wübbenhorst, M. Kemerink and R. P. Sijbesma, *J. Phys. Chem. B*, 2012, **116**, 3928-3937.

19. O. Kotova, R. Daly, C. M. G. dos Santos, P. E. Kruger, J. J. Boland and T. Gunnlaugsson, *Inorg. Chem.*, 2015, **54**, 7735-7741.

20. Y. Zhang, Q. Wang, Y.-J. Xiao, J. Han and X.-L. Zhao, *Polyhedron*, 2012, **33**, 127-136; S. Hasegawa, S. Horike, R. Matsuda, S. Furukawa, K. Mochizuki, Y. Kinoshita and S. Kitagawa, *J. Am. Chem. Soc.*, 2007, **129**, 2607-2614

21. J. Fan, H.-F. Zhu, T.-a. Okamura, W.-Y. Sun, W.-X. Tang† and N. Ueyama, *Chem. Eur. J.*, 2003, **9**, 4724-4731; T. H. Noh, H. Lee, D. Kim, D. Moon, Y.-A. Lee and O.-S. Jung, *Dalton Trans.*, 2016, **45**, 9574-9581; H. Lee, T. H. Noh and O.-S. Jung, *Angew. Chem. Int. Ed.*, 2016, **55**, 1005-1009; J. Park, S. Hong, D. Moon, M. Park, K. Lee, S. Kang, Y. Zou, R. P. John, G. H. Kim and M. S. Lah, *Inorg. Chem.*, 2007, **46**, 10208-10213; D. Moon, S. Kang, J. Park, K. Lee, R. P. John, H. Won, G. H. Seong, Y. S. Kim, G. H. Kim, H. Rhee and M. S. Lah, *J. Am. Chem. Soc.*, 2006, **128**, 3530-3531; P. S. Mukherjee, N. Das and P. J. Stang, *J. Org. Chem.*, 2004, **69**, 3526-3529.

22. X.-M. Zhang, *Coord. Chem. Rev.*, 2005, **249**, 1201-1219; O. R. Evans, R.-G. Xiong, Z. Wang, G. K. Wong and W. Lin, *Angew. Chem. Int. Ed.*, 1999, **38**, 536-538; G. B. Hix, B. M. Kariuki, S. Kitchin and M. Tremayne, *Inorg. Chem.*, 2001, **40**, 1477-1481; K. E. Knope and C. L. Cahill, *Inorg. Chem.* 2008, **47**, 7660-7672; H. L. Dalton, C. S. Hawes and T. Gunnlaugsson, *Cryst. Growth Des.* 2017, **17**, 4365-4376.

23. Y. Ishioka, N. Minakuchi, M. Mizuhata and T. Maruyama, *Soft Matter*, 2014, **10**, 965-971; S. H. Jung, K. Y. Kim, A. Ahn, M. Y. Choi, J. Jaworski and J. H. Jung, *ACS Applied Materials & Interfaces*, 2016, **8**, 14102-14108.

24. R. Sun, Y.-Z. Li, J. Bai and Y. Pan, *Cryst. Growth Des.*, 2007, **7**, 890-894; R. Sun, S. Wang, H. Xing, J. Bai, Y. Li, Y. Pan and X. You, *Inorg. Chem.*, 2007, **46**, 8451-8453.

25. V. A. Blatov, A. P. Shevchenko and D. M. Proserpio, *Cryst. Growth Des.*, 2014, **14**, 3576-3586.

26. G. E. Cmarik, M. Kim, S. M. Cohen and K. S. Walton, *Langmuir*, 2012, **28**, 15606-15613; J. M. Simmons, H. Wu, W. Zhou and T. Yildirim, *Energy & Environmental Science*, 2011, **4**, 2177-2185.

27. Z.-J. Lin, J. Lu, M. Hong and R. Cao, *Chem. Soc. Rev.*, 2014, **43**, 5867-5895; C. S. Hawes, N. F. Chilton, B. Moubaraki, G. P. Knowles, A. L. Chaffee, K. S. Murray, S. R. Batten and D. R. Turner, *Dalton Trans.*, 2015, **44**, 17494-17507.

28. APEX-3, *Bruker-AXS Inc*, 2016, Madison, WI

29. SADABS, *Bruker-AXS Inc*, 2016, , Madison, WI.

30. G. M. Sheldrick, *Acta. Crystallogr. Sect A: Found Adv*, 2015, 3-8; G. M. Sheldrick, *Acta Crystallogr. Sect. C* 2015, 3-8; O. V. Dolomanov, Bouhis, L. J., Gildea, R. J., Howard, J. A. K., Puschmann, H. J., *Appl. Crystallogr.*, 2009, 339-341.

TOC Entry
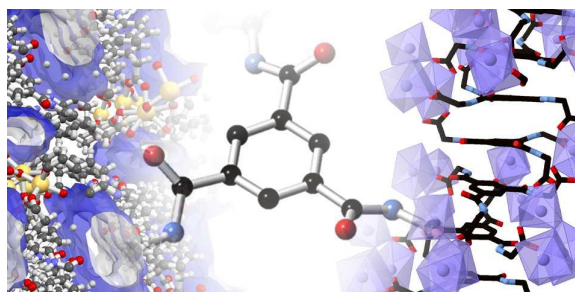
Porous cadmium coordination polymers are prepared from structurally related benzenetricarboxamide ligands, and the functional influence of these scaffolds is examined.

Dalton Transactions Accepted Manuscript